IOP Publishing
Smart Materials and Structures

Smart Mater. Struct. 23 (2014) 015014 (10pp)
doi:10.1088/0964-1726/23/1/015014

Guided wave generation, sensing and damage detection using in-plane shear piezoelectric wafers

Wensong Zhou[1], **Hui Li**[1] **and Fuh-Gwo Yuan**[2]

[1] School of Civil Engineering, Harbin Institute of Technology, Harbin 150090, People's Republic of China
[2] Department of Mechanical and Aerospace Engineering, North Carolina State University, Raleigh, NC 27695, USA

E-mail: yuan@ncsu.edu

Received 7 July 2013, in final form 10 November 2013
Published 10 December 2013

Abstract
This work presents guided wave generation, sensing, and damage detection in metallic plates using in-plane shear (d_{36} type) piezoelectric wafers as actuators and sensors. The conventional lead zirconate titanate (PZT) based on induced in-plane normal strain (d_{31} type) has been widely used to excite and receive guided waves in plates, pipes or thin-walled structures. The d_{36} type of piezoelectric wafer, however, induces in-plane (or called face) shear deformation in the plane normal to its polarization direction. This form of electromechanical coupling generates more significant shear horizontal (SH) waves in certain wave propagation directions, whose amplitudes are much greater than those of Lamb waves. In this paper, an analysis of SH waves generated using in-plane shear electromechanical coupling is firstly presented, followed by a multiphysics finite element analysis for comparison purposes. Voltage responses of both the conventional d_{31} and the new d_{36} sensors are obtained for comparison purposes. Results indicate that this type of wafer has the potential to provide a simple quantitative estimation of damage in structural health monitoring.

Keywords: guided wave, damage detection, in-plane shear, piezoelectric wafer

(Some figures may appear in colour only in the online journal)

1. Introduction

Guided wave based structural health monitoring (SHM) methods have been attracting much attention, mainly due to their capability for long-range and through-the-thickness interrogation of the structures [1–4]. Guided wave SHM methods are based on the elastic stress wave propagation that can be generated and received utilizing transducers in a fairly high frequency range. In contrast to vibration-based global SHM methods, these techniques are sensitive to small structural damage sites or other changes in the structures and can conduct complete distributed monitoring over the entire structure.

In thin plate-like structures, different types of plate (or guided) waves, such as Lamb waves with symmetric and antisymmetric modes, and shear horizontal waves, can be generated by the excitation of piezoelectric materials through electromechanical coupling. When waves encounter discontinuities, such as geometric boundaries, flaws, or damage, they reflect, transmit or scatter, often with additional converted wave modes. It is well known that dispersion and a multi-mode nature are among the inherent properties for Lamb waves. At any excitation frequency, at least two wave modes coexist. Due to wave dispersion, where the phase velocity and group velocity of guided waves depend upon their frequency, the guided waves will become distorted as the propagation distance or time duration increases and further attenuated in amplitude due to geometric spreading. A narrowband signal in a small compact time duration is usually used to generate the guided waves to minimize the influence of the dispersion, yet it still prevails for long propagation distances. One of the solutions is to seek the wave mode which is nearly non-dispersive. Although the wave is still dispersive, the group velocity dispersion curve is fairly flat within a specific frequency range. Another method is to utilize non-dispersive guided waves, such as shear horizontal waves in thin plates or torsional waves in cylindrical structures. However, they can usually only be generated by using a special type of transducer.

In general, Lamb waves can be actively excited and sensed through a number of means. The most commonly used transducers are piezoelectric transducers (piezoelectric wafer, piezoelectric wedge transducer, PVDF and macrofiber composites (MFC), etc), electromagnetic acoustic transducers (EMATs), air-coupled techniques, laser ultrasonics, magnetostrictive transducers, etc. Among them, magnetostrictive transducers (e.g., [5, 6]) and thickness shear mode piezoelectric transducers [7] can readily generate non-dispersive guided waves. However, these two techniques require additional confinement in order to generate such waves, resulting in a larger footprint than conventional piezoelectric wafers. A d_{15} mode PZT was proposed to monitor seismic shear stress in concrete structures [8], but not been used in guided wave technology.

In this work, a new piezoelectric wafer of the d_{36} type to generate and detect the guided waves is proposed for damage detection. In contrast to conventional d_{31} type PZT wafers, where an in-plane normal strain is induced, the d_{36} type of piezoelectric wafers induces in-plane shear deformation in the plane normal to its polarization direction. In thin plate structures, this piezoelectric wafer results in zeroth-order non-dispersive shear horizontal waves, while in cylindrical structures it gives zeroth-order non-dispersive torsional waves in a relatively high frequency range, as opposed to the conventional PZT wafers generating dispersive symmetric and antisymmetric wave modes simultaneously.

In the remaining part of this paper, the materials and in-plane shear deformation mechanism of the proposed piezoelectric wafers will be presented first. A finite element analysis in thin metallic plates is carried out in detail to examine displacement profiles in different directions from different sensing locations. Lastly, to validate the numerical results, guided wave generation, sensing and damage detection using d_{36} type wafers will be verified through experiments.

2. d_{36} material and wafers

The direct piezoelectric effect of the piezoelectric coefficient d_{36} indicates that under external in-plane shear stress σ_{12}, the charge density is induced on a face perpendicular to the poled z-direction. The corresponding converse piezoelectric effect is when the external electric field is applied in the z-direction, and the response is the in-plane shear deformation experienced by the material on the face. This in-plane shear deformation is traditionally introduced by constraining its deformation via the device, which commonly consists of several components, such as magnetostrictive transducers or EMATs, but not simply from a single material, such as piezoelectric ceramics. However, for the conventional piezoelectric materials frequently used, utilizing the in-plane shear deformation induced inherently from the d_{36} effect has not been explored for use in structural health monitoring. In this work, a new type of single crystal, relaxor-$PbTiO_3$ (PT), including $Pb(Mg_{1/3}Nb_{2/3})O_3$–$PbTiO_3$ (PMNT) and $Pb(In_{0.5}Nb_{0.5})O_3 - Pb(Mg_{1/3}Nb_{2/3})O_3 - PbTiO_3$ (PIN–PMN–PT) is poled and then cut in special directions to generate in-plane shear deformation when an electric field is applied along the z-direction, forming a d_{36} type piezoelectric wafer. This type of piezoelectric ceramic has attracted considerable attention over the past two decades, primarily due to its excellent conventional electromechanical properties.

The proposed piezoelectric wafer may be obtained by means of cutting the crystal in a special direction, for example PMNT shown in figure 1(a), in which [*hkl*] in crystallography denotes a direction normal to the plane (*hkl*). The PMNT crystal is first orientated in a Cartesian coordinate system with the crystal growth direction parallel to the z axis. Then the PMNT crystal is poled in the [011] direction and the wafer is cut in the plane (011). The value of the piezoelectric coefficient of [011] poled PMNT28 crystals in the original coordinates (Zhang *et al* [9]), where the piezoelectric d_{31} and d_{32} were found to be 460 and -1188 pC N^{-1} respectively, is given in equation (1)

$$\mathbf{d} = \begin{bmatrix} 0 & 0 & 0 & 0 & 1630 & 0 \\ 0 & 0 & 0 & 239 & 0 & 0 \\ 460 & -1188 & 890 & 0 & 0 & 0 \end{bmatrix} \times 10^{-12}\ \mathrm{C\,N^{-1}} \tag{1}$$

while the elastic compliance matrix is shown as

$$\mathbf{S} = \begin{bmatrix} 14.4 & -23.6 & 15.5 & 0 & 0 & 0 \\ -23.6 & 58.1 & -37.6 & 0 & 0 & 0 \\ 15.5 & -37.6 & 30.5 & 0 & 0 & 0 \\ 0 & 0 & 0 & 14.7 & 0 & 0 \\ 0 & 0 & 0 & 0 & 101 & 0 \\ 0 & 0 & 0 & 0 & 0 & 18.8 \end{bmatrix} \times 10^{-12}\ \mathrm{m^2\,N^{-1}}. \tag{2}$$

The PMNT28 wafer in the original coordinates is shown as the small square with solid boundaries marked in blue lines in figure 1(a). They have the properties matrix given in equations (1) and (2). By rotating the crystal wafer around the new Z axis [011] counterclockwise by an angle θ, the piezoelectric coefficient d'_{36} can be expressed as [10]:

$$d'_{36} = (d_{32} - d_{31})\sin\theta\cos\theta + d_{36}\cos 2\theta. \tag{3}$$

Since d_{36} is zero in the original [011] poled PMNT28 crystals, the above equation is simplified to:

$$d'_{36} = (d_{32} - d_{31})\sin\theta\cos\theta. \tag{4}$$

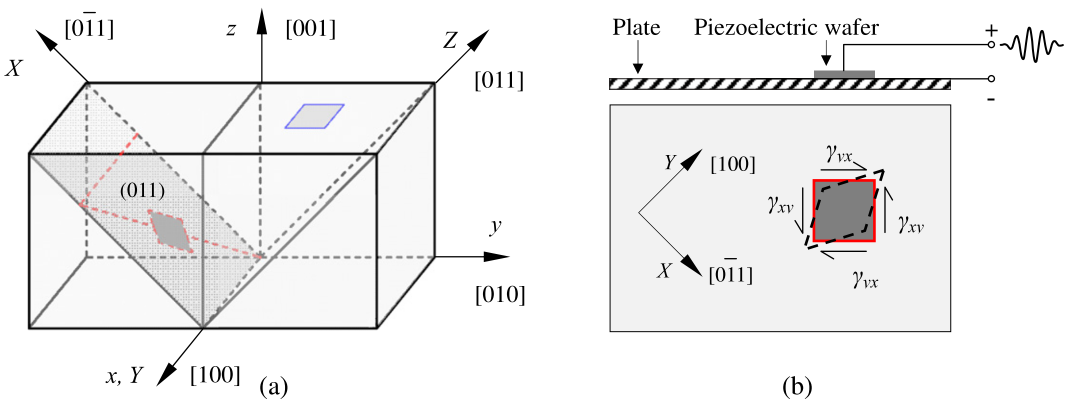

Figure 1. Cutting direction of poled PMNT material and in-plane shear deformation of the PMNT mounted on a plate.

Obviously, the above piezoelectric coefficient reaches its maximum in the $ZXt \pm 45°$ cut direction for the wafer poled along the [011] direction. According to the IEEE Standard on Piezoelectricity [11], the first letter Z indicates the direction of the thickness of the wafer, the second letter X the direction of the length of the wafer, the third letter t denotes the rotation around the thick direction of the wafer, and 45° is the rotation angle. The small square with dashed boundaries marked in red lines in figure 1(a) indicates the original shape and position of a d_{36} type piezoelectric wafer in the PMNT crystal. Figure 1(b) show the deformation of a d_{36} type piezoelectric wafer placed on the surface of a plate and the applied electric field in the poling direction, Z. The deformation can be considered due to a pair of shear strains, γ_{xy} and γ_{yx}.

Finally, after $ZXt45°$ rotation, $d_{36} = d_{32} - d_{31}$ can be derived according to equation (4), and the matrix in equation (1) can be transformed to:

$$\mathbf{d}' = \begin{bmatrix} 0 & 0 & 0 & -696 & 935 & 0 \\ 0 & 0 & 0 & 935 & -696 & 0 \\ -364 & -364 & 890 & 0 & 0 & -1648 \end{bmatrix} \times 10^{-12}\ \mathrm{C\ N^{-1}} \quad (5)$$

where the piezoelectric coefficient d_{36} reaches its maximum, and d_{14} and d_{25} are now present.

The corresponding elastic compliance matrix can be written as:

$$\mathbf{S}' = \begin{bmatrix} 11.0 & 1.64 & -11.0 & 0 & 0 & 21.9 \\ 1.64 & 11.0 & -11.0 & 0 & 0 & 21.9 \\ -11.0 & -11.0 & 30.5 & 0 & 0 & -53.8 \\ 0 & 0 & 0 & 57.7 & -43.0 & 0 \\ 0 & 0 & 0 & -43.0 & 57.7 & 0 \\ 21.9 & 21.9 & -53.8 & 0 & 0 & 120.0 \end{bmatrix} \times 10^{-12}\ \mathrm{m^2\ N^{-1}}. \quad (6)$$

The properties above for the in-plane shear mode of PMNT single crystals have also been evaluated using the impedance method by Zhang *et al* [7]. The experimental data were in good agreement with the rotated matrix calculations and finite element method simulations. Zhang *et al* [12] also investigated the in-plane shear coupling k_{36} and piezoelectric coefficient d_{36} of PMNT crystals as a function of temperature. Moreover, the occurrence of the maximum d_{36} up to 2400 pC $\mathrm{N^{-1}}$ and a large electromechanical coupling factor k_{36} as high as 87% have been theoretically and experimentally confirmed [13]. It should be noted conversely that along the ±45° directions the wafer will experience both extension and compression in-plane normal strains, thus giving rise to symmetric and antisymmetric Lamb wave modes propagating in these directions. As will be shown in section 3, after one or more reflections from the boundaries, the Lamb wave signals will be received by the sensors.

3. Finite element analysis on the plate

To explore wave generation and sensing using the proposed piezoelectric wafer for damage detection, finite element analyses were first conducted on a metallic plate using both the conventional d_{31} type and d_{36} type wafer for comparison purposes. A plate was modeled with ANSYS using a solid185 element, and a d_{36} or a d_{31} type piezoelectric wafer modeled by a solid5 element, which were bonded onto the surface directly (adhesive layer is neglected in the modeling). The plate shown in figure 2 is made of aluminum (Young's modulus $E = 71.0$ GPa, Poisson's ratio $\upsilon = 0.33$ and density $\rho = 2700$ kg $\mathrm{m^{-3}}$) of 1.6 mm in thickness, and 18 cm and 12 cm in length and width respectively. The square-shaped actuator (3 mm × 3 mm) was placed on a location 60 mm away from the edge of the plate, with the plate clamped on all edges. The size of the elements is less than 1/20th of the shortest wavelength among A_0, S_0 and SH_0 waves, while the time step during finite element analysis is chosen according to the center frequency f_c of the excitation signal, i.e. the time step is less than $(1/20)f_c$. Displacement components of a sensing point were extracted from the simulation results. The sensing point is positioned along a long symmetric axis of the plate and located 60 mm from the center of the actuator.

The excitation from the piezoelectric wafer is a 5-cycle sinusoid tone-burst signal enclosed in a Hanning window with a center frequency f_c is kept fixed at 160 kHz. According to results from d_{31} type of PZT, both A_0 and S_0 modes of Lamb waves appear simultaneously under the excitation

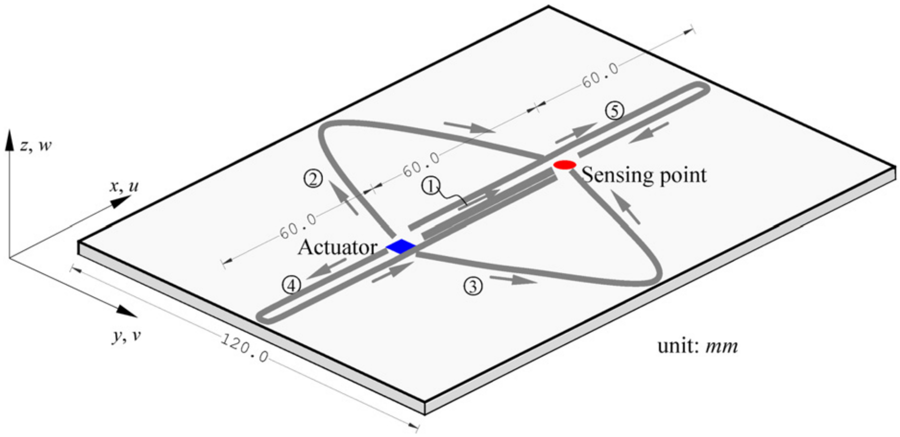

Figure 2. Layout of the piezoelectric wafer and five wave propagation paths from the piezoelectric wafer to the sensing point.

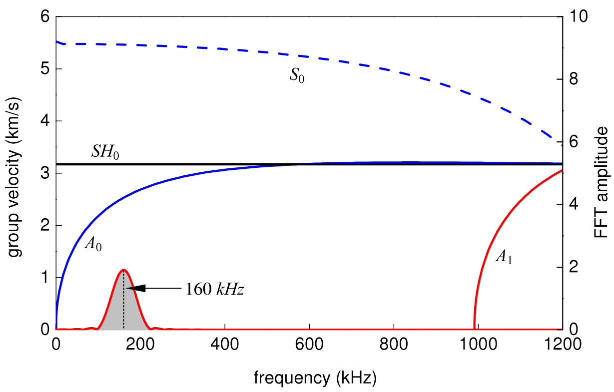

Figure 3. Group velocity of Lamb wave and amplitude spectrum of the excitation signal.

of this frequency. It can be seen through frequency domain analysis that the frequency components for this narrowband signal are mainly concentrated in a small region around the center frequency f_c, thus the dispersive effect can be significantly reduced. The amplitude spectrum of excitation signal was plotted together with group velocity dispersion curves corresponding to three wave modes in figure 3.

3.1. Displacement field in the three-dimensional model

To highlight wave generation using a d_{36} type piezoelectric wafer, the relatively small values of piezoelectric coefficients related to the induced in-plane normal deformation are intentionally removed from the piezoelectric material matrix in equation (4). Figure 4 shows the snapshots of the displacement contours on the surface of the plate in three directions, and the total displacement contour, excited by the d_{36} actuator at the time 22 μs respectively. The waves in figures 4(a) and (b) are the displacement contours in the x and y directions respectively. They can be identified as the shear horizontal waves, since the waves travel along the y and x directions, whereas the particle displacement is along x and y respectively. Moreover, since the shear horizontal waves emitted from each side of the square-shaped piezoelectric wafer cover a moderate range of angles, implying that the coverage of the shear horizontal waves lies outside the x and y axes. In figure 4(c), the particle displacement in the z axis propagates mainly in the 45° direction with respect to the symmetric axis of the wafer. That is, Lamb waves travel in this direction. However, they are of much smaller magnitude along the both 0° and 90° directions, because along these two directions shear horizontal waves are dominant. Figure 4(d) shows the total displacement field on the surface of the plate. In contrast, the displacement distributions with the d_{31} type wafer (PZT-5H) are shown as figure 5. It is obvious that the particle motion is parallel to the direction of wave propagation, at the same time all the material particle disturbance has components in the z direction, typical of classical Lamb waves. In addition, from figure 4, the displacements of the d_{36} type wafer following the symmetry and antisymmetry can be expressed as

$$u(x, y) = u(-x, y), \qquad v(x, y) = v(x, -y) \quad \text{and} \quad w(x, y) = w(-x, -y) \tag{7a}$$

$$u(x, y) = -u(x, -y), \qquad v(x, y) = -v(-x, y) \quad \text{and} \quad w(x, y) = -w(x, -y) = -w(-x, y). \tag{7b}$$

But for the d_{31} type wafer, the displacements shown in figure 5 follow the symmetry and antisymmetry

$$u(x, y) = -u(-x, y), \qquad v(x, y) = -v(x, -y) \quad \text{and} \quad w(x, y) = w(-x, -y) \tag{8a}$$

$$u(x, y) = u(x, -y), \qquad v(x, y) = v(-x, y) \quad \text{and} \quad w(x, y) = w(x, -y) = w(-x, y). \tag{8b}$$

3.2. Finite element analysis of plate waves excitation with d_{36} actuator

Figure 6 shows three displacement components at the sensing point, 60 mm away from the actuator. The range of the y axis is kept fixed to illustrate their relative magnitudes. As shown in the figure, the displacement in the y direction is much more significant than those in the x and z directions. The first five wave traveling paths are indicated with gray lines in figure 2, and listed in table 1 with the group velocities of A_0

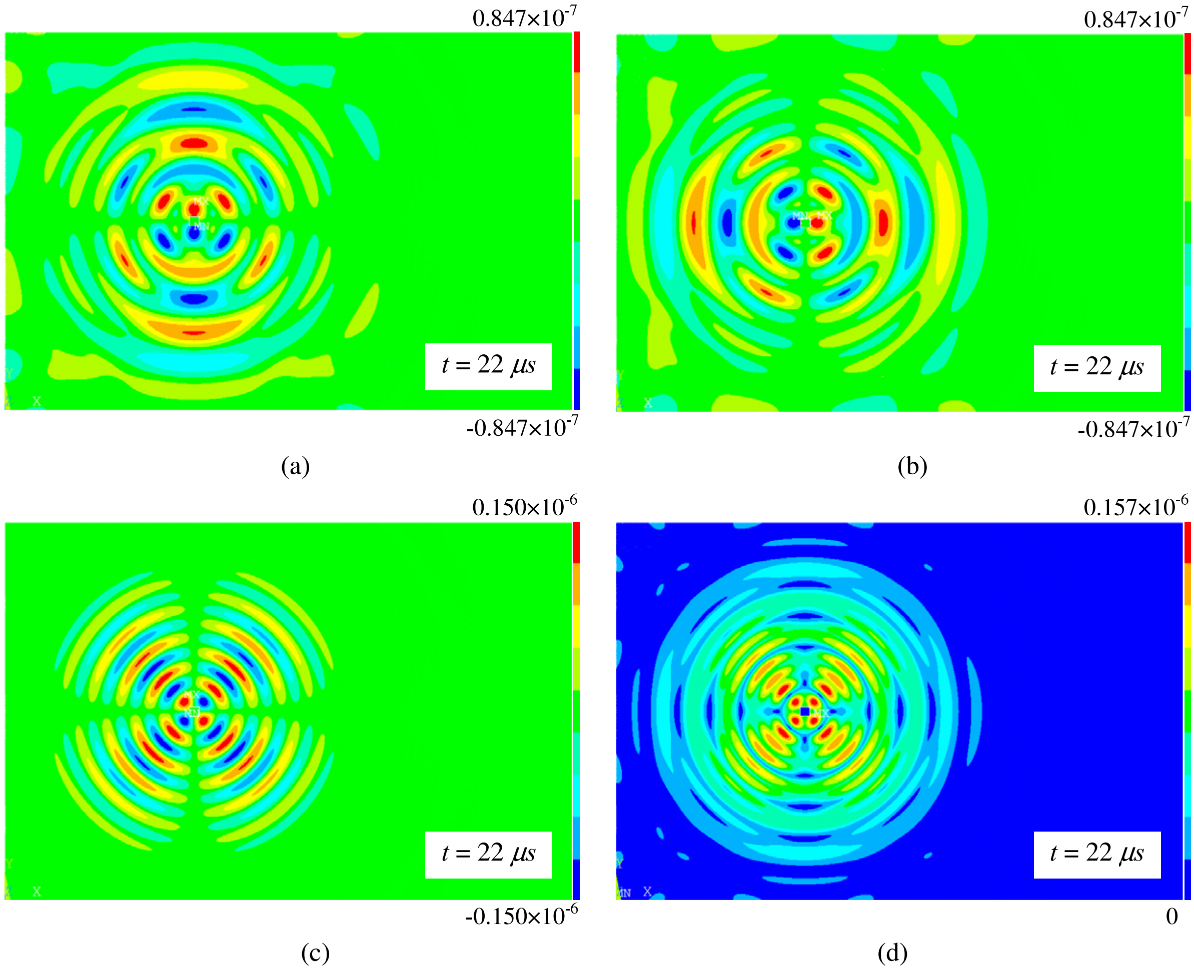

Figure 4. Displacement contour under excitation of a d_{36} type piezoelectric wafer: (a) displacement contour u in the x direction. (b) Displacement contour v in the y direction. (c) Displacement contour w in the z direction. (d) Total displacement contour.

Table 1. Time of arrival of guided waves at 160 kHz in the aluminum plate (unit: μs).

	A_0	S_0	SH_0
Group velocity (m s^{-1})	2460	5338	3040
Path ① (60.0 mm)	24.39	11.24	19.74
Paths ② and ③ (134.1 mm)	54.51	25.13	44.11
Paths ④ and ⑤ (180.0 mm)	73.17	33.72	59.21

and S_0 Lamb waves and the SH_0 wave. All the times of arrival were estimated as table 1. From the wave velocities and the displacement contours in figure 4, the in-plane displacement v in the wavepackets shown in figure 6 can be identified as the direct and reflected SH_0 waves, from wavepaths ①, ②, ③, ④ and ⑤. Of which, the SH_0 waves along paths ② and ③ are emitted directly from the side of the wafer in the y direction. The transverse displacement w in the wavepacket is the superposed reflected A_0 waves from paths ② and ③. Thus along wavepaths ② and ③, the A_0 and SH_0 wave modes coexist.

These preliminary results indicate that the d_{36} type piezoelectric wafer is capable of generating shear horizontal waves in appropriate directions.

3.3. Displacement responses due to the crack

Additional numerical simulations are implemented with respect to cracks with different orientations to investigate the feasibility of damage detection using the d_{36} type wafer. Since the zeroth-order shear horizontal wave is non-dispersive, the pulse wave signals received from the sensor are easier to recognize from their wave propagation paths. A through-the-thickness crack with two different orientations is created on the finite elements model between the wafer and the detection point, shown as figure 7. The dimension of the crack is 18.0 mm long by 1.2 mm wide.

The exact same wafers and excitation signals were used in these two simulation studies. Results for the vertical crack are shown as figure 8. Both displacements u and w have much smaller amplitude than the displacement v. As shown in figure 8(b), for the direct path from the actuator to the sensor (No. ①) the displacement v (in y direction) is affected greatly, because the vertical crack obstructs the propagation of waves even when the particle moves along the crack orientation. For the reflected paths (Nos. ② and ③), the waveform is affected little, since the paths do not pass the crack. In addition, for these paths, there is phase difference between the

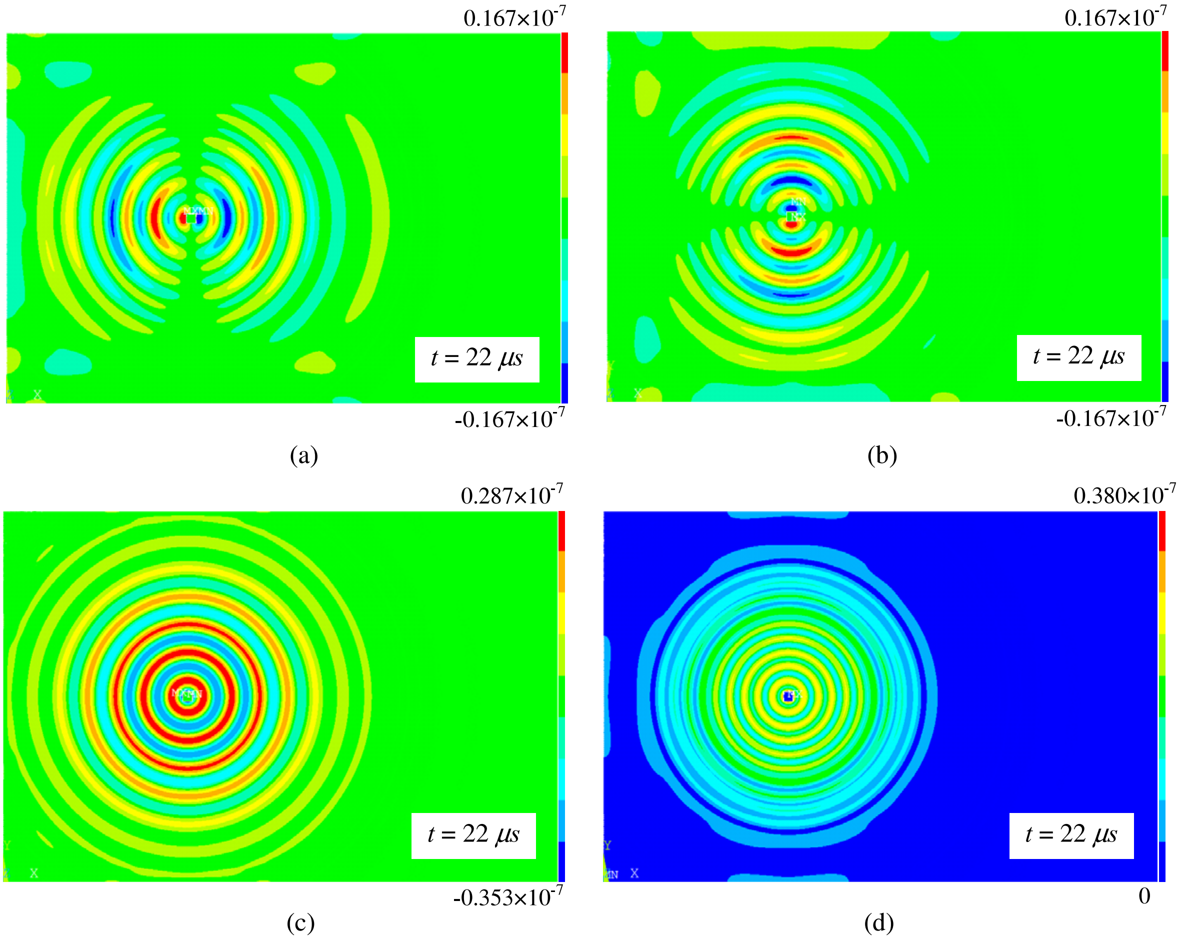

Figure 5. Displacement contour under excitation of a d_{31} type piezoelectric wafer: (a) displacement contour u in the x direction. (b) Displacement contour v in the y direction. (c) Displacement contour w in the z direction. (d) Total displacement contour.

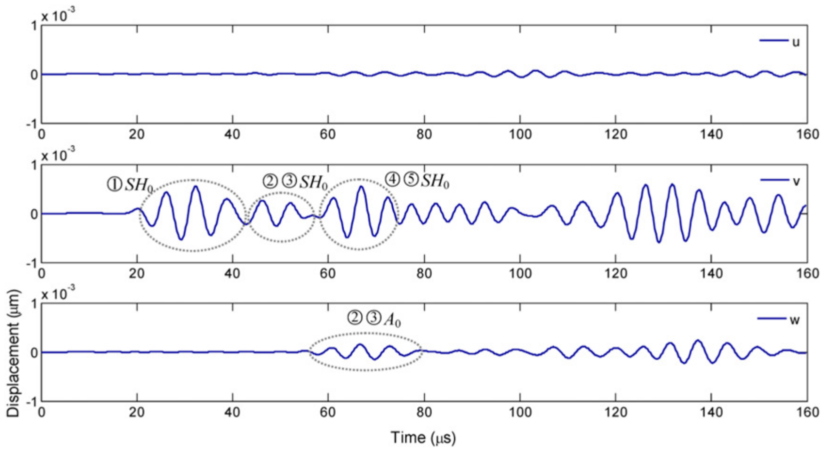

Figure 6. Displacement responses at the sensing point (numerical simulation).

displacement responses for cases with and without the crack; this results from the interference from the crack. Moreover, because the reflected paths Nos. ④ and ⑤ pass through the crack, the displacement v in the y direction also decreases.

For the parallel crack, results are shown in figure 9. For the direct wave path (No. ①), the displacement v in the y direction has been slightly modified in magnitude and phase. For reflected wave paths (Nos. ② and ③), the phenomenon is similar; however, for reflected wave paths (Nos. ④ and ⑤), the magnitude is significantly reduced and the phase is almost out of phase due to the crack.

4. Experimental studies on the plate

A series of experiments was designed to demonstrate guided wave generation, sensing and damage detection using

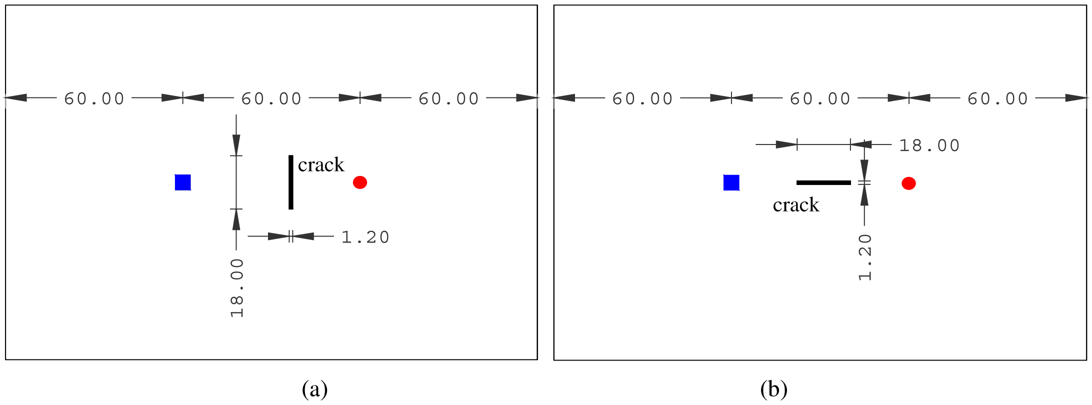

Figure 7. The location and orientation of cracks on the plate: (a) crack length perpendicular to the pulse-catch direction (vertical crack). (b) Crack length parallel to the pulse-catch direction (parallel crack).

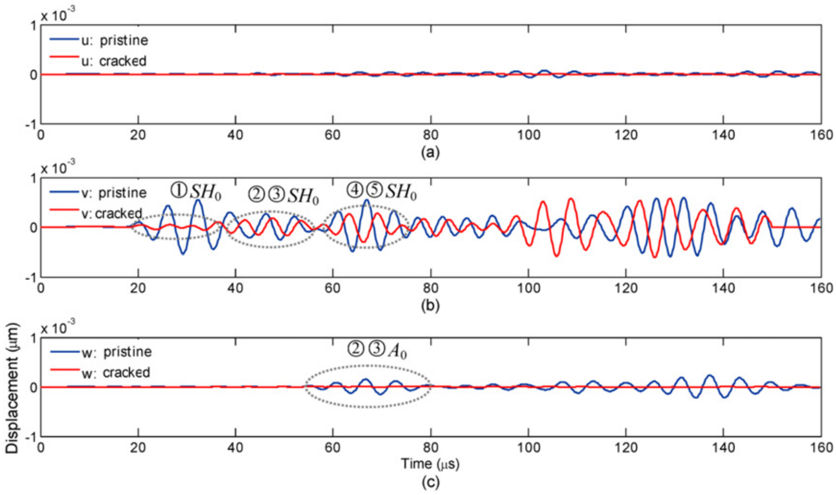

Figure 8. Displacement responses to a vertical crack (numerical simulation).

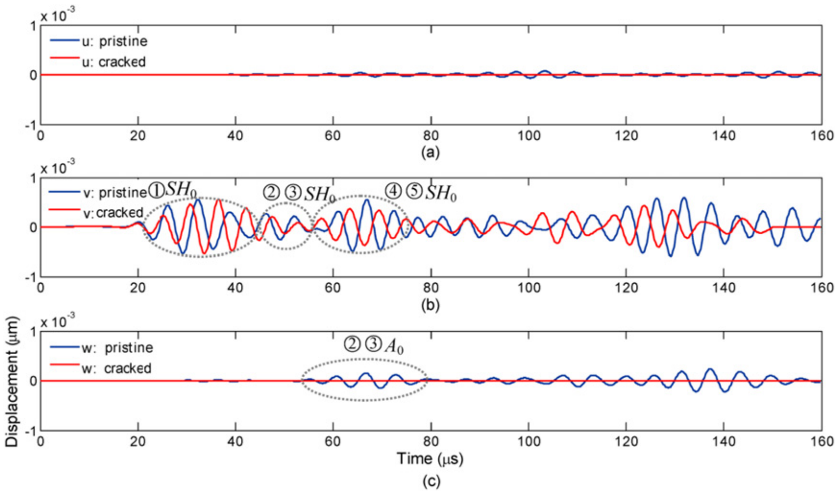

Figure 9. Displacement responses to a parallel crack (numerical simulation).

d_{36} piezoelectric wafers. A pair of wafers is mounted on the top surface of an aluminum plate (Al-6061 with 914.4 mm × 914.4 mm × 1.6 mm). The size of the wafer as both actuator and sensor is 9 mm × 9 mm × 0.5 mm. This thin wafer can reduce the effect of the induced bending moment applied to the plate from the wafer. Superglue, which may form a very thin and stiff adhesive layer, was used to attach these wafers on the plate. The actuator was

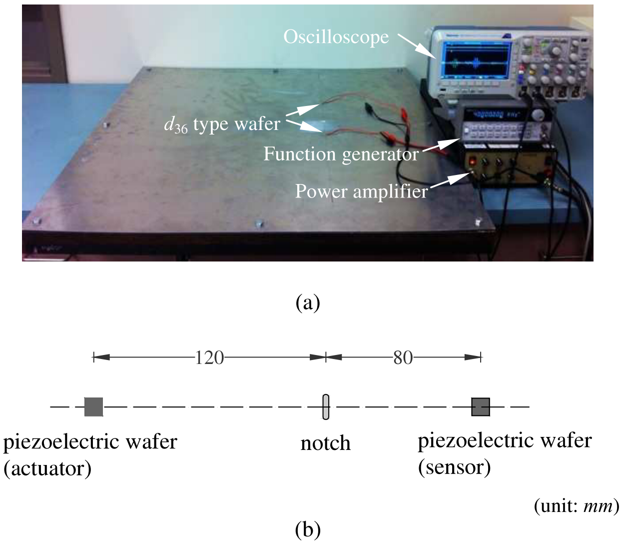

Figure 10. Experimental setup for the generation and sensing of guided waves.

driven by a function generator (HP 33 210 A), into which a five-peaked wave signal was preprogrammed. Its amplitude and center frequency can be changed during the test. A wideband (DC-1 MHz) power amplifier (Krohn-Hite-7602) was used to amplify the excitation voltage. The signal induced from the sensor was collected by a digital oscilloscope (DPO 2024, Tektronix, Inc.). Figure 10(a) is the actual photo of the experimental setup. In the experiment, one of three wafers was used as the actuator, and another was used as the sensor. Their layout and location are shown in figure 10(b). The distance between all wafers and the boundary of the plate is about 30 cm.

4.1. Experimental results on the pristine plate

The center frequency of the excitation signal f_c is varied from 40 to 200 kHz in increments of 40 kHz. The signals collected by the sensor are shown as figure 11. For all figures, the amplitudes of the excitation signals were kept fixed at 30 V_{pp}. According to the group velocity of S_0, A_0 and SH_0 modes, they all can be recognized in the voltage response curves. For 40 and 80 kHz excitations, S_0 mode Lamb waves are difficult to capture due to their very small amplitude, while the amplitude of the A_0 mode Lamb waves becomes smaller beyond 80 kHz and interferes with SH_0 mode waves, since their group velocities are becoming closer, making them easier to see in figure 3. Due to the large piezoelectric coefficient, the amplitudes of SH_0 remain large for most of the test cases. Moreover, from the beginning time of SH_0 waves, it can be found that their velocities keep constant for all frequencies of excitation. All results show that the PMNT piezoelectric wafer is able to generate and sense SH_0 waves.

4.2. Experimental results on the notched plate

In real structures, damage is located at arbitrary locations in different geometries. In this work, for preliminary investigation purposes, a simple vertical notch, shown as figure 10(b), was cut by an endmill to simulate the damage in the plate. The notch was first cut 3 mm wide by 10 mm long, and 0.8 mm deep (half the thickness of the plate). Figure 12 shows the experimental results of the pristine and damaged plate respectively and their differences. As the excitation frequency increases from 40 to 200 kHz; that is, the wavelength reduces from 76 to 15 mm, the amplitude of transmission SH_0 waves decreases in this frequency range. To quantify the degree to which transmission is affected by the damage, a transmission coefficient is defined as the peak amplitude change in the first SH_0 wave time arrival to that in the pristine state. The transmission coefficient is shown in figure 13 for different excitation frequencies accompanied by the corresponding reflection coefficient [14, 15].

5. Conclusions and recommendations

In this paper, a new piezoelectric wafer made of PMNT material is proposed to generate and sense guided waves, and

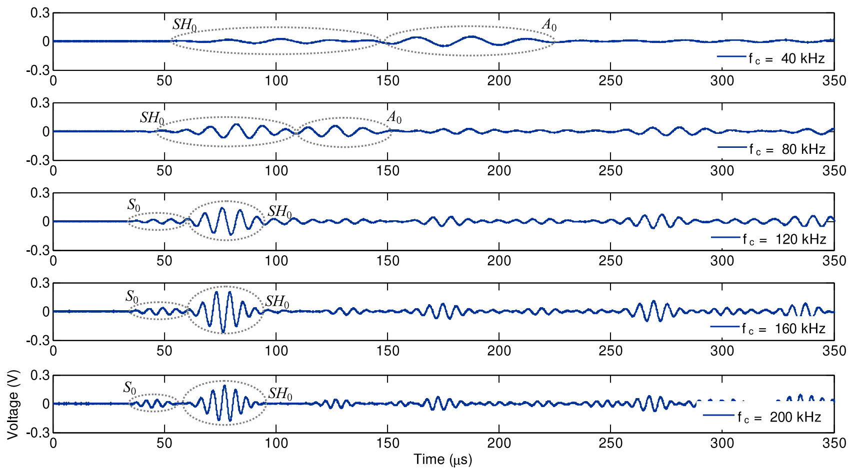

Figure 11. Sensor output voltage for different central frequencies (experimental results).

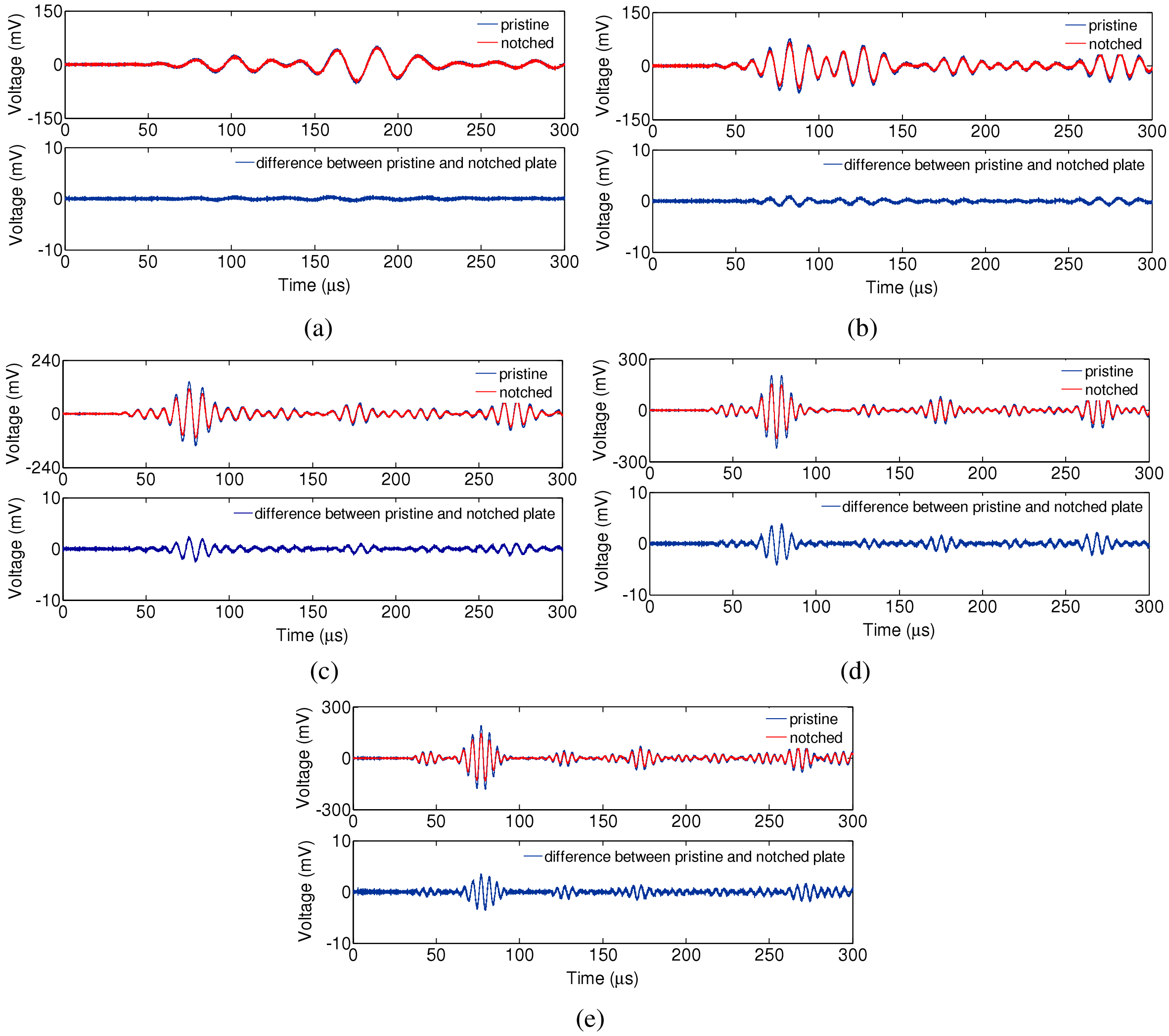

Figure 12. Sensor output voltages for the pristine and notched plate and their difference: (a) 40 kHz. (b) 80 kHz. (c) 120 kHz. (d) 160 kHz. (e) 200 kHz.

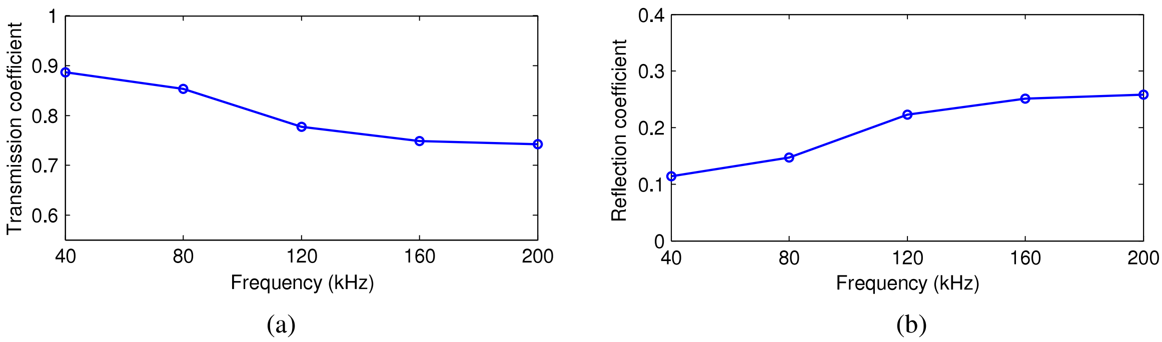

Figure 13. Transmission and reflection coefficients: (a) transmission coefficient. (b) Reflection coefficient.

also further used to explore its capability to detect damage. With a specific cutting direction, a very large d_{36} piezoelectric coefficient is present in the piezoelectric matrix of this kind of piezoelectric wafer—at the same time the d_{31} and d_{32} coefficients are also present with relatively smaller values. This wafer can be used to generate SH waves with large amplitudes and symmetric and antisymmetric mode Lamb waves with small amplitudes. The single non-dispersive SH_0 wave mode is observed from both displacement contours and response curves for excitation frequencies below the first cut-off frequency of the dispersion curve for shear horizontal waves. Meanwhile, FEM results also show that the SH_0 waves are capable of detecting damage along their propagation paths.

Subsequently, experiments on an aluminum plate with attached PMNT wafers were conducted to demonstrate the practicability of guided wave generation, sensing and guided wave based damage detection using the proposed wafers. In the experimental results, the amplitude of the SH_0 mode waves is larger than the other wave modes with respect to some frequencies. For pulse-catch experiments with the notch perpendicular to the direct wave propagation path, as the excitation frequencies increase, the amplitudes of transmission of SH_0 waves decrease in the frequency range studied. The reduction of transmitted signals may be used to quantify the structural damage. Theoretical and detailed parametric analyses on quantifying the damage will be the topic of future investigations.

Acknowledgments

The financial support from the National Key Technology R&D Program under Grant No. 2011BAK02B02, and the National Science Foundation of China under Grant No. 50908066 is gratefully appreciated.

References

[1] Rokhlin S 1980 Diffraction of Lamb waves by a finite crack in an elastic layer *J. Acoust. Soc. Am.* **67** 1157–65
[2] Cawley P and Alleyne D 1996 The use of Lamb waves for the long range inspection of large structures *Ultrasonics* **34** 287–90
[3] Raghavan A and Cesnik C E S 2007 Review of guided-wave structural health monitoring *Shock Vib. Dig.* **39** 91–114
[4] Song G, Gu H, Mo Y L, Hsu T T C and Dhonde H 2007 Concrete structural health monitoring using embedded piezoceramic transducers *Smart Mater. Struct.* **16** 959–68
[5] Kwun H and Teller C M 1994 Magnetostrictive generation and detection of longitudinal, torsional, and flexural waves in a steel rod *J. Acoust. Soc. Am.* **96** 1202–4
[6] Light G M, Kwun H, Kim S Y and Spinks R L Jr 2003 Health monitoring of piping and plate using the magnetostrictive sensor (MsS) guided-wave technology *Proc. 2nd Mid. E. NDT Conf. Exhib. (Jubail Industrial City, Saudi Arabia)*
[7] Liu Z, He C, Wu B, Wang X and Yang S 2006 Circumferential and longitudinal defect detection using T(0,1) mode excited by thickness shear mode piezoelectric elements *Ultrasonics* **44** e1135–8
[8] Hou S, Zhang H and Ou J 2013 A PZT-based smart aggregate for seismic shear stress monitoring *Smart Mater. Struct.* **22** 065012
[9] Zhang S, Jiang W, Meyer R J Jr, Li F, Luo J and Cao W 2011 Measurement of face shear properties in relaxor-$PbTiO_3$ single crystals *J. Appl. Phys.* **110** 064106
[10] Yan W, Han P and Jiang Z 2012 Piezoelectric 36-shear mode for [011] poled 24%$Pb(In_{1/2}Nb_{1/2})O_3$–$Pb(Mg_{1/3}Nb_{2/3})O_3$–$PbTiO_3$ ferroelectric crystal *J. Appl. Phys.* **111** 034107
[11] American National Standards Institute 1988 *IEEE Standard on Piezoelectricity: Std 176-1987* (Piscataway, NJ: IEEE)
[12] Zhang S, Li F, Jiang W, Luo J, Meyer R J Jr, Cao W and Shrout T R 2011 Face shear piezoelectric properties of relaxor-$PbTiO_3$ single crystals *Appl. Phys. Lett.* **98** 1829903
[13] Han P 2004 Piezoelectric crystal elements of shear mode and process for preparation *US Patent* 7,908,722 B2
[14] Ratassepp M, Fletcher S and Lowe M J S 2010 Scattering of the fundamental torsional mode at an axial crack in a pipe *J. Acoust. Soc. Am.* **127** 730–40
[15] Demma A, Cawley P, Lowe M J S and Roosenbrand A G 2003 The reflection of the fundamental torsional mode from cracks and notches in pipes *J. Acoust. Soc. Am.* **114** 611–25